J. Fluid Mech. (1964), *vol.* 20, *part* 1, *pp.* 47–79
Printed in Great Britain

Convection in a radiating gas

By JOHN GILLE AND RICHARD GOODY
Harvard University

(Received 23 March 1964)

We have made a theoretical and experimental study of the effect of radiative transfer on the onset of convection by means of comparative experiments in dry air and ammonia contained between horizontal aluminium plates maintained at different temperatures.

The first effect of radiative transfer is to distort the linear, diffusive profile in the initial, pre-convective state. A non-grey theory is developed and is shown to predict the non-linear profiles with satisfactory accuracy. The change of radiative flux with pressure of ammonia is also predicted and confirmed. This constitutes the first successful attempt to confirm the methods used in atmospheric studies in controlled experiment.

A non-grey theory of the onset of convection is developed, separating effects associated with the distortion of the static state and the dissipative effect of radiative transfer on temperature fluctuations.

Experiments indicate that the critical Rayleigh number in ammonia can be greatly increased over the best value for air ($Ra_c = 1786$); the maximum observed being $Ra_c = 4870$. Theory and experiment are shown to agree within reasonable limits.

This work confirms the validity of methods which are of great importance to astrophysics and atmospheric physics.

CONTENTS

1. Introduction

The onset of convection in a radiating fluid constitutes one of the simplest closed convection problems of relevance to astrophysics and geophysics. Solutions for a grey absorbing gas (absorption independent of wavelength) contained between two horizontal surfaces have been given by Goody (1956) and Spiegel

(1960). The radiation has a stabilizing effect which depends strongly on the scale of the phenomenon, being large for geophysical and astrophysical scales but small for laboratory scales. Goody (1956) suggested that the small effects predicted for the scale of a few centimetres might be detected in the laboratory, and we have made experiments to verify this prediction.

The apparatus consists of two horizontal plates, whose temperatures can be controlled independently (see §6), containing between them gaseous ammonia. The large dipole moment and low moment of inertia of this molecule combined to give ammonia an emissivity comparable to water vapour, without the same upper limit on the vapour pressure at laboratory temperatures.

Although our main concern was with the onset of convection, it is evident that we first had to understand the initial static state. In the first place, the temperature profile is not linear, which influences the onset conditions. In the second place, the heat flux for ammonia is pressure dependent, and, since we use pressure changes to vary the conditions for the onset of convection and heat flux to indicate the onset itself, the connexion between them has to be understood.

In §§2–7 the methods used to compute temperature profiles and heat fluxes for a non-grey gas are discussed, and compared with experiment. They are analogous to methods used in planetary atmospheres, but in natural systems it is extremely difficult to compare prediction and observation with certainty because of unsteady conditions and unaccounted constituents such as dust and haze. The relatively simple conditions of our laboratory experiment, therefore, permit us to make a much more satisfactory evaluation of the theoretical methods than has heretofore been possible. In §§8–12 we shall develop an approximate non-grey theory of the onset of convection in ammonia and describe an experimental verification of the theory.

2. The optical properties of ammonia

In §§4 and 5 the theoretical problem will be stated in terms of the function

$$\mathscr{E}(r) = \int_0^\infty Q_\nu(1 - e^{-k_\nu r})\, d\nu \Big/ \int_0^\infty Q_\nu d\nu, \tag{1}$$

where $Q_\nu = dB_\nu/d\theta$, B_ν is Planck's black-body function, θ the temperature, ν the frequency, k_ν the volume absorption coefficient, and r the path length.

Laboratory measurements of emissivity (see Hottel 1954) yield the quantity

$$E(r) = \int_0^\infty B_\nu(1 - e^{-k_\nu r})\, d\nu \Big/ \int_0^\infty B_\nu d\nu. \tag{2}$$

The general form of B_ν does not differ greatly from that of Q_ν, and (1) and (2) are therefore similar quantities. There is, however, no way of going directly from one to the other without consideration of some details of k_ν. Moreover, we find that the derivative $\mathscr{E}'(r)$ is needed with considerable accuracy. The empirical data on $E(r)$ cannot, however, be differentiated with acceptable precision without also considering some details of k_ν. Although our knowledge of the detail of k_ν is extensive, it is not by itself sufficient to give the required data with sufficient accuracy. We therefore adopt the following procedure, which is analogous to that employed for meteorological problems (see, e.g., Goody 1964).

From consideration of the absorption spectrum and available data on line-widths and intensities we construct for a number of ranges the statistical parameters

$$y = \alpha/\delta, \quad u = Sr/2\pi\alpha, \tag{3}$$

where α represents the Lorentz line-width, S the line intensity, δ is the mean line spacing $= \Delta\nu/N$, where $\Delta\nu$ is the frequency width of range, and N the number of lines in the range.

The mean transmission for the ith range can then be estimated from the statistical model for a single line intensity

$$\bar{T}_i = \exp -\{2\pi y_i L(u_i)\}, \tag{4}$$

where

$$L(u_i) = u_i e^{-u_i}\{I_0(u_i) + I_1(u_i)\}$$

is the Ladenberg and Reiche function, which has been tabulated by Kaplan & Eggers (1956). This is only one of a group of models which might equally well be employed; in view of our method of normalization the choice is not of critical importance.

Since Q_ν and B_ν vary little over the chosen spectral ranges, we may write

$$\mathscr{E}(r) = \frac{\Sigma_i Q_i\{1 - \bar{T}_i(r)\}\Delta\nu_i}{Q}, \tag{5}$$

$$E(r) = \frac{\Sigma_i B_i\{1 - \bar{T}_i(r)\}\Delta\nu_i}{B}, \tag{6}$$

where Q and B denote quantities integrated over all frequencies.

$E(r)$ can be computed for the case of ammonia diluted by N_2 at a total pressure of one atmosphere, and compared with Port's (1940) data, as presented by Hottel (1954). Using the best available spectrographic data, a small discrepancy, averaging about 8 % of the emissivity, remained. We found that this discrepancy could be resolved if we added the effect of 150 lines each of intensity 0·125 cm^{-2}. Such a line intensity is close to the lower limit recorded spectrographically, and the total added intensity is less than 3 % of the total band intensity for ammonia. Thus, the discrepancy between theory and measurement can be removed by the presence of a few lines, whose presence can neither be affirmed nor denied.

The band model parameters can now be recomputed for the line-widths appropriate to pure ammonia, at a variety of pressures and hence (5) can be evaluated. $\mathscr{E}'(r)$ can also be evaluated directly from the band model using the derivative of (4). By this means we may expect to obtain $\mathscr{E}(r)$ and $\mathscr{E}'(r)$ with the same precision that is demonstrated for $E(r)$, that is, to within $\pm 2\,\%$, approximately.

The vibration-rotation bands of ammonia are shown in figure 1. The most important feature is the strong group of ν_2 bands (932 and 968 cm^{-1}) stretching from 650 to 1265 cm^{-1}. According to McKean & Schatz (1956) this band has a total intensity of 600 cm^{-1} $(\text{atm. cm})^{-1}$. The ν_4 band at 1628 cm^{-1} stretches from 1324 to 1940 cm^{-1}, and has, according to the same authors, an intensity of 110 cm^{-1} $(\text{atm. cm})^{-1}$, where both measurements are presumed to be at room temperature.

The ν_1 and ν_3 fundamentals near 3400 cm^{-1} are of negligible importance to our problem, and apart from the rotation band only the upper state band $(2\nu_2 - \nu_2)$ need be considered. It was assumed that transition probabilities for this band were the same as for the fundamental.

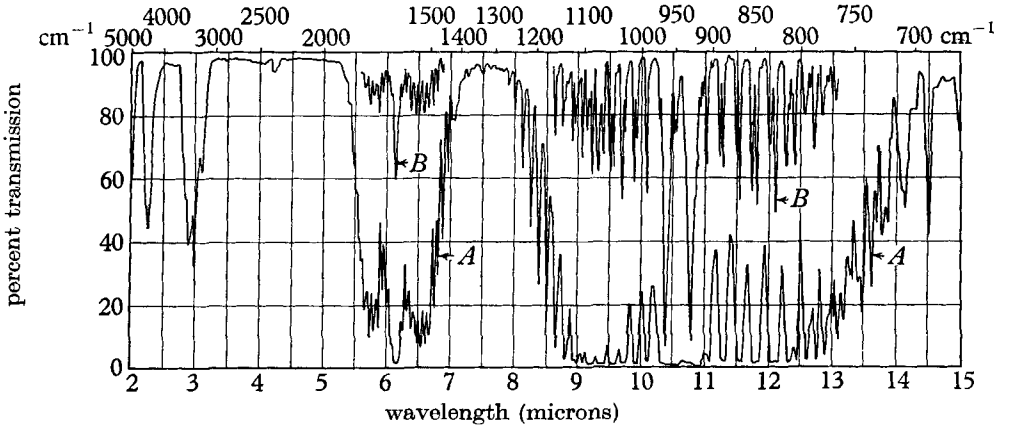

FIGURE 1. A low resolution absorption spectrum of ammonia (after Pierson, Fletcher & Gantz 1956). The rotation spectrum is not shown. Curve *A*, p_{NH_3} = 700 mmHg; curve *B*, p_{NH_3} = 45 mmHg. Cell length 10 cm.

The ν_2 fundamental was divided into seven regions: the antisymmetric Q branch (aQ); the symmetric Q branch (sQ); the region between the Q branches (I); strong and weak portions of the P branch ($P(s)$ and $P(w)$); strong and weak portions of the R branch ($R(s)$ and $R(w)$). The $(2\nu_2^s - \nu_2^a)$ transition was treated in two parts: the P and Q branches combined ($2aP$, $2aQ$); and the R branch ($2aR$) combined with $P(w)$, which it overlaps. The $(2\nu_2^a - \nu_2^s)$ falls in the centre of the ν_2 band and can be neglected. The ν_4 band is treated as a single region.

Details of the parameters used are given in table 1. The division of band intensity between ranges in the ν_2 and $(2\nu_2 - \nu_2)$ bands is based on the theoretical line strengths of Benedict, Plyler & Tidwell (1958). The frequency ranges are based upon the observed spectra of Garing, Nielsen & Rao (1959). The same source is used to give the number of lines in the ν_2 band ranges, but the theoretical work of Benedict *et al.* was used for the ν_4 and $(2\nu_2 - \nu_2)$ bands.

The rotation band of ammonia can only absorb about 3 % of room temperature black-body rotation for very long path lengths. We have treated each J-group of $(2J+1)$ lines as a separate spectral region. Intensities were deduced from Gerhard & Dennison (1933), and Foley & Randall (1941), while the widths of J groups were obtained from Wright & Randall (1933), Slawsky & Dennison (1939), Hansler & Oetjen (1952), Foley & Randall (1941), and Hadni (1953).

It now remains to assign a value to the Lorentz line-width at one atmosphere pressure, both for ammonia broadened by dry nitrogen (α_{N_2}) and for self-broadening by ammonia (α_{NH_3}). Widths are a function of both quantum numbers J and K, but the ratio $\alpha_{NH_3}/\alpha_{N_2}$ is likely to be less variable than the widths themselves. We have adopted $\alpha_{NH_3}/\alpha_{N_2} = 8{\cdot}0$, on the basis of microwave measurements cited by Hirschfelder, Curtiss & Bird (1954).

The line-width for a mixture of nitrogen and ammonia can now be written

$$\alpha(p) = (p_0)^{-1}(p_{NH_3} + p_{N_2}/8)\,\alpha_{NH_3}(p_0), \tag{7}$$

where p_{NH_3} and p_{N_2} are the partial pressures of ammonia and nitrogen, respectively.

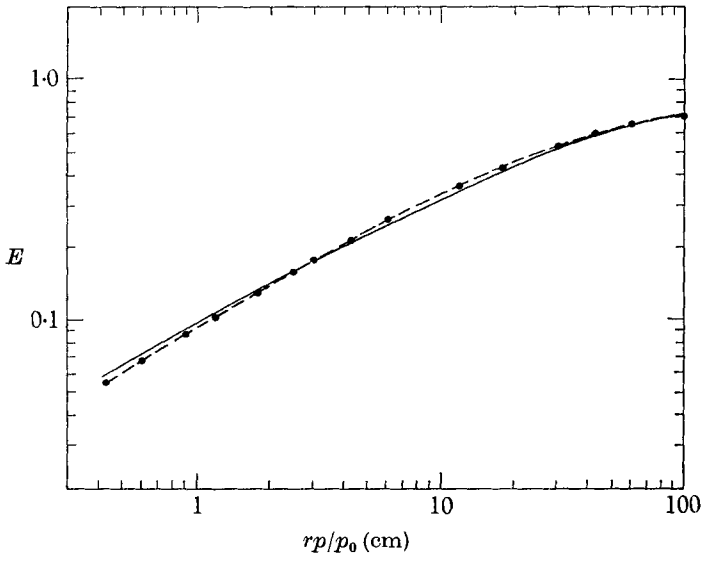

FIGURE 2. The emissivity of ammonia in dilute mixture with nitrogen at one atmosphere pressure and 300 °K. (rp/p_0) is the virtual path of pure ammonia, reduced to standard pressure. The full line is calculated. The broken line is observed.

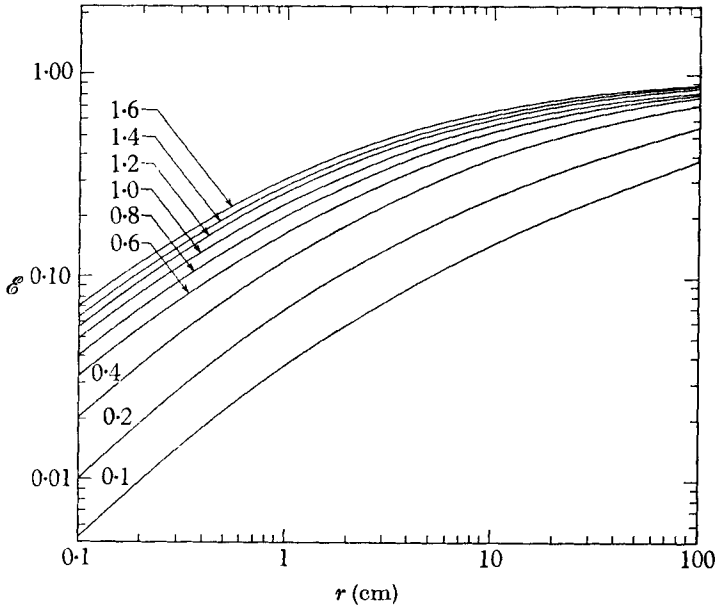

FIGURE 3. $\mathscr{C}(r)$ for pure ammonia at 300 °K. Numbers on curves are pressures in atmospheres.

Benedict *et al.* (1958) have measured line widths for ammonia self-broadening in the combination band ($\nu_2+\nu_3$). For four lines measured by three different methods they found α_{NH_3} (S.T.P.) = 0·42 cm^{-1}. The same (JK) lines in the microwave rotation spectrum have been measured with greater accuracy (Bleaney

Range	Frequency [cm^{-1}]	$\Delta\nu$ [cm^{-1}]	Range intensity $A = NS$ [cm^{-1} (atm. cm)$^{-1}$]	N	S [cm^{-1} (atm. cm)$^{-1}$]	$\delta = \frac{\Delta\nu}{N}$ [cm^{-1}]
aQ	910–945	35	114·8	52	2·207	0·67
I	945–952	7	7·8	11	0·708	0·64
sQ	952–970	18	118·9	45	2·642	0·40
$P(s)$	785–910	125	106·2	59	1·800	2·12
$P(w)$, $2aR$	648–785	137	11·3	141	0·081	0·97
$R(s)$	970–1123	153	224·1	51	4·394	3·0
$R(w)$	1123–1265	142	26·4	70	0·377	2·03
ν_4	1324–1940	616	11·0	549	0·200	1·12
$2aQ$, $2aP$	325–647	322	1·9	194	0·010	1·66

TABLE 1. Range parameters for ammonia.

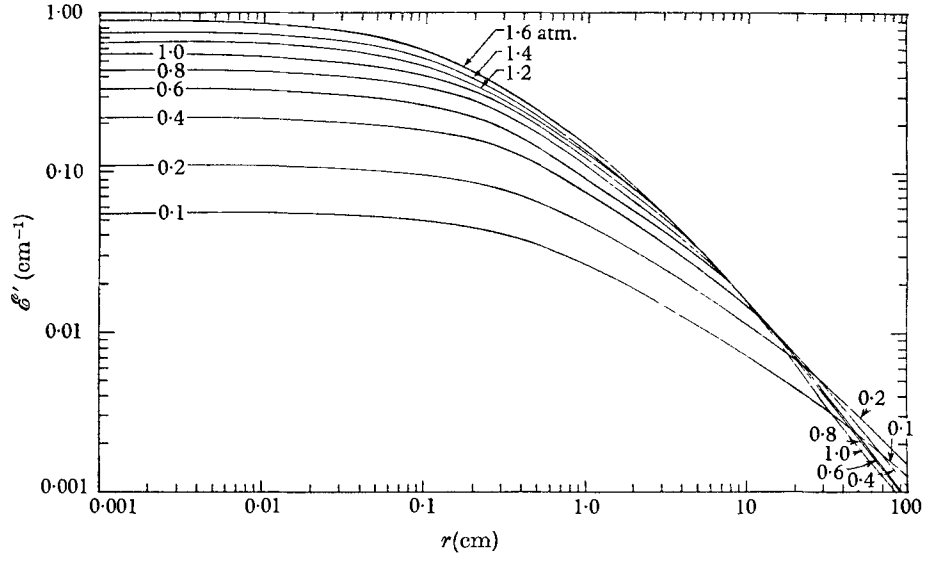

FIGURE 4. $\mathscr{E}'(r)$ for pure ammonia at 300 °K. Numbers on curves are pressures in atmospheres.

& Penrose 1948): α_{NH_3} (S.T.P.) = 0·52 cm^{-1}. We have adopted the latter figure, on the grounds of the greater precision of measurement. Our normalization procedure ensures that our results will not depend critically on the choice.

Good agreement between observed and theoretical emissivities for ammonia mixed with air is indicated in figure 2. Using the same spectrographic data we have computed $\mathscr{E}(r)$ and $\mathscr{E}'(r)$, and the results are shown in figures 3 and 4.

3. The physical properties of air and ammonia

We require the following physical data: K (thermal conductivity); η (viscosity); $c_p, c_v, \rho(p, \theta)$ (density as a function of pressure and temperature); n (the refractive index) for both air and ammonia. It turns out that the accuracy needed to interpret our measurements is slightly greater than that to which these quantities are presently known.

Air

Apart from the refractive index, all the relevant properties for air are reviewed in the National Bureau of Standards (1955*a*) publication *Tables of thermal properties of gases*. The value of K used here is $2{\cdot}63 \times 10^3$ erg cm^{-1} sec^{-1} (°K)$^{-1}$ at 300 °K, without pressure dependence, but varying nearly as $\theta^{\frac{1}{2}}$. The spread of experimental results upon which these data are based is about $\pm 2\,\%$ for η and $\pm 4\,\%$ for K.

Ammonia

The first virial coefficient for ammonia is known with sufficient accuracy. We have employed the gas law

$$\frac{p}{\rho r\theta} = 1 + B\rho, \tag{8}$$

where r is the gas constant per gramme. The value of B was taken from Hirschfelder *et al.* (1954).

$c_p(p, \theta)$ has been measured with great accuracy by Osborne, Stimson, Sligh, & Crague (1924), and Thompson (1941) has shown excellent agreement with spectrographic data. c_v was then obtained from the relation

$$c_p - c_v = r + 2\,(dB/d\theta)\,p. \tag{9}$$

The viscosity of ammonia varies greatly with temperature, but there appears to be no comparable variation with pressure. We have employed the data of van Cleave & Maass (1935).

According to Chapman & Cowling (1952) we may write

$$K(p, \theta) = f\eta(\theta)\, c_v(p, \theta), \tag{10}$$

where, according to Mason & Monchick (1962), f is a constant. From a measurement of K at 240 mmHg and 0 °C by Franck (1951) we find that $f = 1{\cdot}47$, and thence $K(p, \theta)$ can be computed under any other desired conditions. K changes by about $1{\cdot}75\,\%$ between $p = 0$ and 760 mmHg; its value at 300 °K and zero pressure is taken to be $2{\cdot}44 \times 10^3$ erg cm^{-1} sec^{-1} (°K)$^{-1}$, with a temperature factor close to $\theta^{\frac{1}{2}}$. We tentatively estimate the errors in these data to be the same as for air.

The ratio $(c_p g\alpha/K\eta)\rho^2$

The non-dimensional Rayleigh number, required in § 8, involves the fundamental physical data in the form of the ratio $c_p g\alpha\rho^2/K\eta$ where

$$\alpha = -\rho^{-1}\partial\rho/\partial\theta \tag{11}$$

is the coefficient of expansion, determined numerically from the gas laws. Figure 5 gives this ratio as a function of temperature and pressure for both air and ammonia. (The factor $(p_0/p)^2$ has been included to take account of the effect of pressure upon ρ^2.)

Refractive indices

The refractive index for dry air is a well determined quantity and is quoted, for example, in Landholt & Bornstein (1962). For the Mercury green line at 15 °C and 760 mmHg pressure,

$$n(15; 760) - 1 = 2{\cdot}77901 \times 10^{-4}.$$

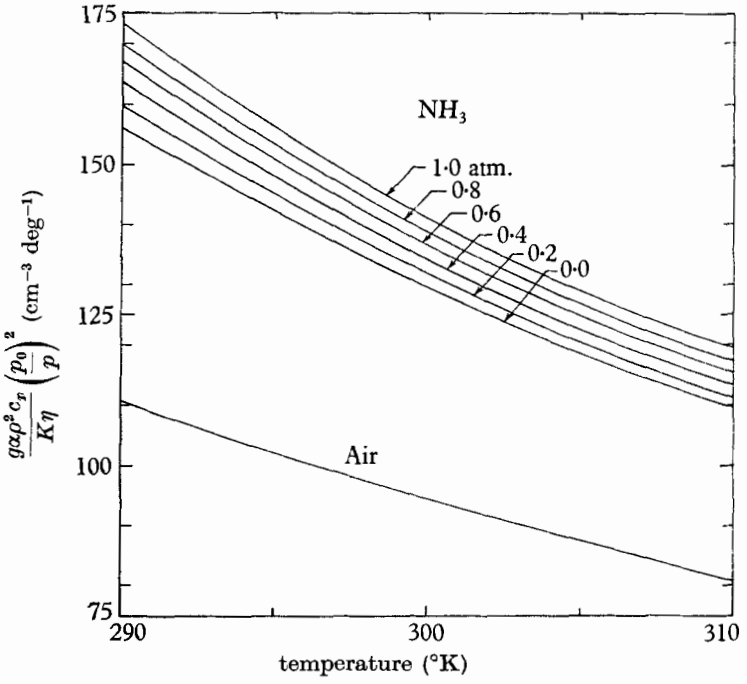

FIGURE 5. $g\alpha c_p \rho^2/K\eta\,(p_0/p)^2$ for air and ammonia.

Uncertainty in the experimental data for ammonia is more the result of the method of reduction to S.T.P. than of the measurement of refractive index. Friberg (1927) makes clear his method of reduction and we have therefore adopted his value at 5462 Å.

$$n(0; 760) - 1 = 3{\cdot}8442 \times 10^{-4}.$$

Other measurements cited by Landholt & Bornstein either agree with this value, or are not fully explicit as to the method of reduction.

4. Calculation of the temperature profile

In these experiments either ammonia or dry air was contained between two horizontal aluminium alloy plates spaced apart by 2 or 5 cm. Air does not interact with the radiation flux and a linear temperature profile will result. Since the plates are not mirrors, however, a large radiative heat flux passes directly from one plate to the other. Ammonia on the other hand absorbs and re-emits radiation from the plates, and the resulting interaction between radiation and molecular diffusion gives rise to a non-linear temperature profile.

To illustrate the general nature of the phenomenon we may quote the result for grey radiation (absorption coefficient, k, per unit volume). Using the Eddington approximation to allow for the diffuse nature of the radiation field, we find (Goody 1964)

$$\frac{\beta}{\bar{\beta}} = \frac{\chi\cosh(g\tau - \frac{1}{2}gkh) + \cosh(\frac{1}{2}gkh) + (g/2m)\sinh(\frac{1}{2}gkh)}{(2\chi/gkh)\sinh(\frac{1}{2}gkh) + \cosh(\frac{1}{2}gkh) + (g/2m)\sinh(\frac{1}{2}gkh)}, \tag{12}$$

where $$g = \sqrt{\{3(1+\chi)\}}, \quad \chi = \frac{4\pi Q}{3\overline{K}k}, \quad \tau = kz,$$

z is the vertical co-ordinate, h the plate separation, $m = (2-\epsilon)/\epsilon$, ϵ the emissivity of plates, β the temperature gradient $\partial\theta/\partial z$, $\bar{\beta} = \Delta\theta/h$ and $\Delta\theta$ the temperature difference between the plates.

Equation (12) gives an S-shaped profile with boundary layers whose characteristic scale length is $\{3k^2(1+\chi)\}^{-\frac{1}{2}}$. The departure from linearity tends to zero as $k \to 0$ or ∞, and a maximum departure exists for some finite density of absorbing gas.

In the case of a non-grey gas no such simple result is available, but numerical computations can be made in terms of the function $\mathscr{E}(r)$.

Let us suppose that the plate emissivities are not functions of the frequency of the radiation. This is not an entirely satisfactory assumption, but we were not able to measure the spectral variation of emissivity, and computation would be greatly complicated if such variation were included. The specific radiation intensity for the case of the thermodynamic equilibrium can be written (see, e.g., Goody 1964)

$$I_\nu^+(\phi,z) = \epsilon B_\nu(0)\exp\{-k_\nu z/|\cos\phi|\} + (1-\epsilon)I_\nu^-(\phi,0)\exp\{-k_\nu z/|\cos\phi|\} + \int_0^z B_\nu(z')\,k_\nu\exp\{-k_\nu(z-z')/|\cos\phi|\}\frac{dz'}{|\cos\phi|}, \tag{13}$$

$$I_\nu^-(\phi,z) = \epsilon B_\nu(h)\exp\{-k\nu(h-z)/|\cos\phi|\} + (1-\epsilon)I_\nu^+(\phi,h)\exp\{-k_\nu(h-z)/|\cos\phi|\} + \int_z^h B_\nu(z')\,k_\nu\exp\{-k_\nu(z'-z)/|\cos\phi|\}\frac{dz'}{|\cos\phi|}, \tag{14}$$

where the $(+)$ and $(-)$ indices represent upward and downward travelling radiation respectively, and ϕ is the angle to the vertical. The three contributions on the right-hand side are respectively emission from the boundary, reflexion from the boundary and emission from the gas lying between z and the boundary.

Provided that the range of temperature is small, and that the two boundaries have the same thermal properties, both θ and B are anti-symmetric about the centre of the gas. We can make use of this information to separate equations (13) and (14). Evaluate equation (13) at $z = h$ and (14) at $z = 0$, add the two equations, and from the symmetry condition, we find the invariant relation

$$I_\nu^+(h) + I_\nu^-(0) = B_\nu(h) + B_\nu(0). \tag{15}$$

Hence we find

$$I_\nu^+(\phi,z) = B_\nu(z) + \int_0^z \frac{\partial B_\nu(z')}{\partial z'}\exp\{-k_\nu(z-z')/|\cos\phi|\}\,dz' + \frac{(1-\epsilon)\exp\{-k_\nu z/|\cos\phi|\}}{1+(1-\epsilon)\exp\{-k_\nu h/|\cos\phi|\}}\int_0^h \frac{\partial B_\nu(z')}{\partial z'}\exp\{-k_\nu(k-z')/|\cos\phi|\}\,dz'. \tag{16}$$

The flux of radiation is given by

$$F_\nu(z) = \int_0^\pi 2\pi \cos\phi \sin\phi I_\nu(\phi, z)\, d\phi,$$

involving integrals of the kind

$$R(x) = \int_0^\pi 2\pi \cos\phi \sin\phi \exp\{-x/|\cos\phi|\}\, d\phi,$$

which we replace approximately by $R(x) \simeq \pi e^{-sx}$, where s is known as the diffusivity factor. This approximation is widely used in the meteorological literature, and has been shown to be good for $s = 1{\cdot}667$.

We now find

$$F_\nu^+(z) = \pi B_\nu(z) - \int_0^z \frac{\partial \pi B_\nu(z')}{\partial z'} \exp\{-sk_\nu(z-z')\}\, dz' + \frac{(1-\epsilon)\exp\{-sk_\nu z\}}{1+(1-\epsilon)\exp\{-sk_\nu h\}} \int_0^h \frac{\partial \pi B_\nu(z')}{\partial z'} \exp\{-sk_\nu(h-z')\}\, dz', \quad (17)$$

$$F_\nu^- = \pi B_\nu(z) + \int_z^h \frac{\partial \pi B_\nu(z')}{\partial z'} \exp\{-sk_\nu(z'-z)\} dz' - \frac{(1-\epsilon)\exp\{-sk_\nu(h-z)\}}{1+(1-\epsilon)\exp\{-sk_\nu h\}} \int_0^h \frac{\partial \pi B_\nu(z')}{\partial z'} \exp\{-sk_\nu z'\} dz'. \quad (18)$$

The radiative heating rate is

$$H_r = -\int_0^\infty \frac{d}{dz}(F_\nu^+(z) - F_\nu^-(z))\, d\nu. \quad (19)$$

Since we are dealing with a small range of temperature we may write

$$dB_\nu = Q_\nu d\theta, \quad (20)$$

and treat Q_ν as a constant. In the third terms of (17) and (18) expand the denominator in a power series, and then introduce

$$\mathscr{E}'(r) = Q^{-1} \int_0^\infty Q_\nu k_\nu e^{-k_\nu r}\, d\nu, \quad (21)$$

into the resulting expression for the heating rate. We find

$$H_r = \pi s Q \Big[-\int_0^z \beta(z')\, \mathscr{E}'(s[z-z'])\, dz' + \int_z^h \beta(z')\, \mathscr{E}'(s[z'-z])\, dz' + (1-\epsilon)\int_0^h \beta(z') \times \{[\mathscr{E}'(s[h+z-z']) - \mathscr{E}'(s[h+z'-z])] - (1-\epsilon)[\mathscr{E}'(s[2h+z-z']) - \mathscr{E}'(s[2h+z'-z])] + (1-\epsilon)^2 [\mathscr{E}'(s[3h+z-z']) - \mathscr{E}'(s[3h+z'-z])] - \ldots\}\, dz' \Big]. \quad (22)$$

If heat is simultaneously diffused, the resulting steady state is given by

$$H_r + K\frac{\partial \beta(z)}{\partial z} = H(z) = 0. \quad (23)$$

There are a number of different techniques available for solving (22) and (23) for $\beta(z)$. We have chosen to make an expansion in a manner suggested by the 'grey' solution (12),

$$\beta(\zeta)/\bar{\beta} = A + B\zeta^2 + C\zeta^4 + D\zeta^6 \ldots, \tag{24}$$

where $\zeta = (z/h) - \frac{1}{2}$. Symmetry requires that the odd terms are absent from (24).

ζ	Three coefficients in equation (24)	Four coefficients in equation (24)
0·0	0·0000	0·0000
0·1	0·0226	0·0260
0·2	0·0432	0·0469
0·3	0·0565	0·0565
0·4	0·0498	0·0480
0·5	0·0000	0·0000

TABLE 2. $-\left(\dfrac{\theta-\bar{\theta}-\zeta\Delta\theta}{\Delta\theta}\right)$ for pure ammonia. $h = 5{\cdot}048$ cm; $p_{NH_3} = 30{\cdot}4$ cm Hg; $\epsilon = 0{\cdot}352$.

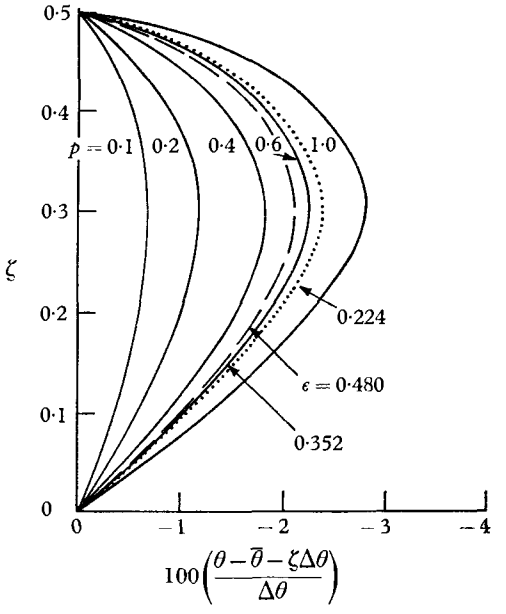

FIGURE 6. $100\,(\theta-\bar{\theta}-\zeta\Delta\theta)/\Delta\theta$ for pure ammonia; $h = 1{\cdot}987$ cm, $\epsilon = 0{\cdot}352$, and pressures in atmospheres as marked on the curves. The broken and dotted curves are for $p_{NH_3} = 0{\cdot}6$ atm., $\epsilon = 0{\cdot}480$ and $0{\cdot}224$, respectively.

For each pressure, a table of $\mathscr{E}'$ is available. If we substitute (24) into (22), we may compute H in terms of A, B, C, D, etc., for sufficient values of ζ to provide the number of simultaneous equations needed to evaluate these coefficients. Since the average value of the left-hand side of (24) is unity, one relation between the coefficients is immediately available; thus if we wish to determine a three-term expansion, the heating rate must be determined at two points in the gas. By symmetry, $H = 0$ at $\zeta = 0$, and this result is assured by the expansion (24).

Thus the points of evaluation must be at ζ other than zero; for a three-term expansion we have chosen to evaluate the integrals at $\zeta = 0{\cdot}3$ and $0{\cdot}5$.

In table 2 we have compared computations using three and four coefficients in equation (24). The data used ($h = 5\,\text{cm}$, $p = 30{\cdot}4\,\text{cmHg}$) were expected to lead to the strongest boundary layers likely to occur in our experiments. The quantity tabulated is the fractional deviation from a linear profile ($\Delta\theta$ = temperature difference between plates, $\bar{\theta}$ = mean temperature). For $\Delta\theta = 7\,^{\circ}\text{K}$

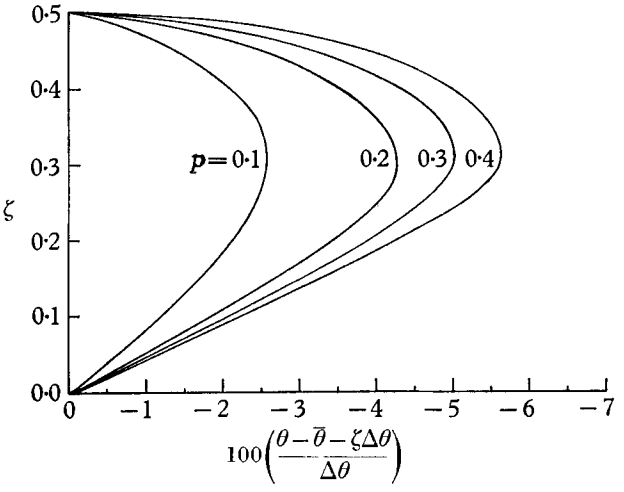

FIGURE 7. $100(\theta-\bar{\theta}-\zeta\Delta\theta)/\Delta\theta$ for pure ammonia; $h = 5{\cdot}048$ cm, $\epsilon = 0{\cdot}352$, and pressures in atmospheres as marked on the curves.

the maximum difference is $2{\cdot}6 \times 10^{-2}\,^{\circ}\text{K}$, which is only just detectable with our equipment. From this we concluded that a three-coefficient expansion was sufficient for our purposes.

For our profile measurements ϵ lies between $0{\cdot}3$ and $0{\cdot}5$; it was therefore sufficient to evaluate only five terms in the expansion in $(1-\epsilon)$, and only the first two had to be evaluated by numerical quadrature. Calculated profiles for pure ammonia and two plate separations are shown in figures 6 and 7. In figure 6 the effect of varying ϵ is illustrated for $p = 0{\cdot}6$ atm.

5. Calculation of the flux

Of the total heat flux between the plates in our experiment, a considerable part comes from thermal conduction and most of the remainder is caused by direct radiation from the hot to the cold plate. Only a small part is absorbed and re-emitted by the ammonia, and, therefore, likely to vary with the amount of this gas between the plates. The variation is, however, significant for the determination of the onset of convection, and is an interesting phenomenon in its own right.

Using the Eddington approximation for a grey-absorbing gas, a complete solution can be made from the equations quoted by Goody (1964) and the result (12) for the temperature gradient. If

$$F = F_r + F_c \tag{25}$$

is the total heat flux, where F_r is the radiative heat flux and F_c the conductive heat flux, we find

$$-\frac{F}{K\beta} = \frac{K_{\text{eff}}}{K} = \frac{1+\chi^{-1}}{\{\frac{1}{2}khg\coth\frac{1}{2}khg + \frac{1}{4}m^{-1}khg^2\}^{-1}+\chi^{-1}}, \tag{26}$$

where K_{eff} is the effective conduction coefficient which might be deduced from an experiment if radiative and conductive effects are not distinguished.

In figure 8 equation (26) is plotted for a number of values of the emissivity. It is understandable that, as the absorption coefficient per unit volume increases indefinitely, the effective conductivity will eventually decrease to the molecular

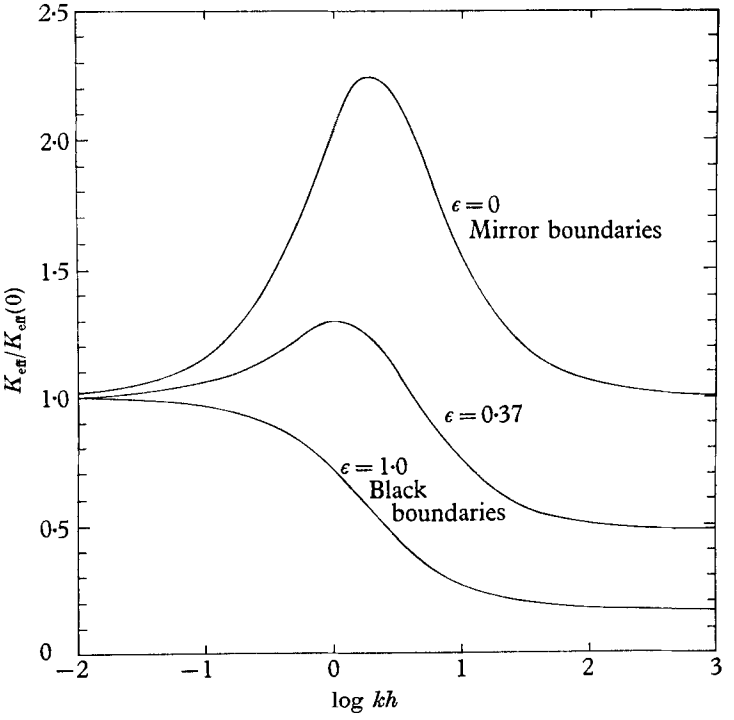

FIGURE 8. Effective conduction coefficient for a grey absorbing gas.

value. The initial increase of K_{eff} for low emissivities is less expected, but can be interpreted if we consider the case $\epsilon = 0$ (mirror boundaries). For $kh = 0$ there is no radiative transfer between the two plates, and $K_{\text{eff}} = K$. A small amount of absorbing gas will not help to transfer heat from the boundaries to the gas, but it will transfer heat more rapidly through the gas itself than would otherwise be possible. An initial increase of K_{eff} with kh is therefore expected.

In terms of equation (26) our experiments correspond to small values of kh, and $K_{\text{eff}}/K_{\text{eff}}(0)$ varies only slightly. We have developed a computational scheme which concentrates attention on this small variation. We can write (25) in the form

$$F = F_r - K\beta. \tag{27}$$

Since F is constant through the fluid, we may take an average value of the right-hand side and write

$$F = \bar{F}_r - K\Delta\theta/h. \tag{28}$$

Starting from equations (17) and (18) and employing the same approximations as in the previous section, we find

$$\bar{F}_r = \frac{2(2-\epsilon)\pi Q}{sh}\int_0^h \beta(z')\,[\tilde{\mathscr{E}}(sz') - (1-\epsilon)\,\tilde{\mathscr{E}}(s\{z'+h\}) + (1-\epsilon)^2\,\tilde{\mathscr{E}}(s\{z'+2h\}) \\ \ldots(-1)^n(1-\epsilon)^n\,\tilde{\mathscr{E}}(s\{z'+nh\})\ldots]\,dz' - \frac{\pi Q\epsilon\Delta\theta}{2-\epsilon}, \qquad (29)$$

where

$$\tilde{\mathscr{E}}(r) = \int_0^r \mathscr{E}(x)\,dx.$$

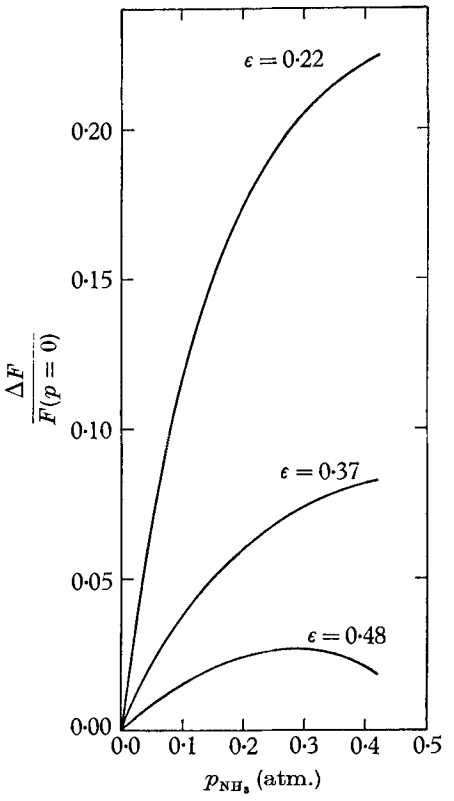

FIGURE 9. $\Delta F/F(p = 0)$ for pure ammonia; $h = 1{\cdot}987$ cm.

The second term on the right-hand side of (29) is simply the flux in the limit of a completely transparent atmosphere. The series in the first term is very slowly convergent, but the remainder after six or seven terms can be evaluated analytically on the basis that $\tilde{\mathscr{E}}(r)$ varies linearly with r for large values of the argument.

Figures 9 and 10 show computations of the flux for two plate spacings and three emissivities. In the course of these computations it became apparent that the results depended greatly upon the gas emissivity data. Moreover, individual computed points differed considerably and erratically from the curves shown. We are of the opinion that the computations reflect real physical effects. It is probable that small changes in emissivity will indeed cause large variations in the observed flux increment, and it is quite possible that the curves have a fine

structure associated with the maxima of figure 8, corresponding to different absorption bands in the spectrum. Such detail is, however, unlikely to be properly rendered by our simple model of the absorption spectrum, and we have therefore been content to draw smooth curves through somewhat scattered points.

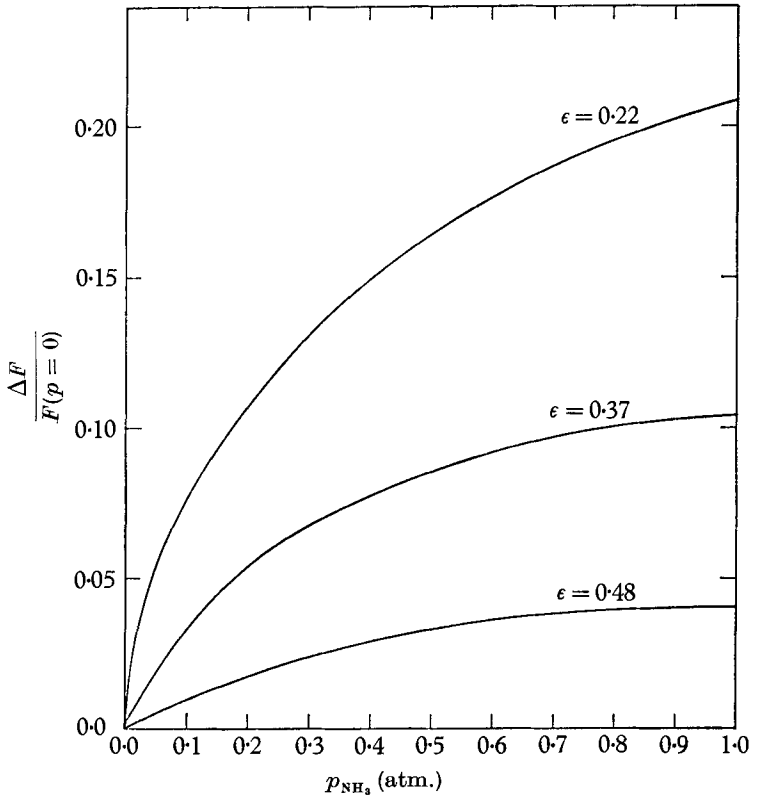

FIGURE 10. $\Delta F/F(p = 0)$ for pure ammonia; $h = 5{\cdot}048$ cm.

6. Apparatus

6.1. *The convection cell*

The cell (see figure 11) consists of a 10 in. diameter (more precisely 25·34 cm) multiple sandwich with two brass plates (0·5 in. thick) on the outside enclosing two nylon plates (0·625 in. thick), two aluminium plates (0·5 in. thick), and the gap to contain air or ammonia, which was held open by three phenolic spacers, either 2 or 5 cm long (more precisely $1{\cdot}987 \pm 0{\cdot}002$ cm and $5{\cdot}048 \pm 0{\cdot}006$ cm). Surfaces of all plates were accurately machined and special attention was paid to the two inward facing aluminium surfaces which, after assembly, were explored with a surface gauge and shown to be flat to within $\pm$ 0·001 in. The brass plates were soldered to doubly wound spirals of copper tubing, which were covered with phenolic plates to minimize heat loss. The whole sandwich was contained inside a Plexiglass sleeve, and placed inside a sealed chamber made of aluminium alloy. The Plexiglass sleeve was pierced by two holes and optical glass flats were inserted in the sealed chamber at opposite ends of a diameter for the purpose of admitting one arm of a Michelson interferometer (see §6.3).

Temperature control was effected by passing water from thermostated baths through the two brass plates at the rate of 0·31 min^{-1}. The two streams entered the sealed chamber through nylon seals to avoid thermal contact with the chamber, but left through metal seals. The water supplies were held thermostatically to about ± 0·01 °K and an attempt was made to keep the average temperature of the two baths close to room temperature.

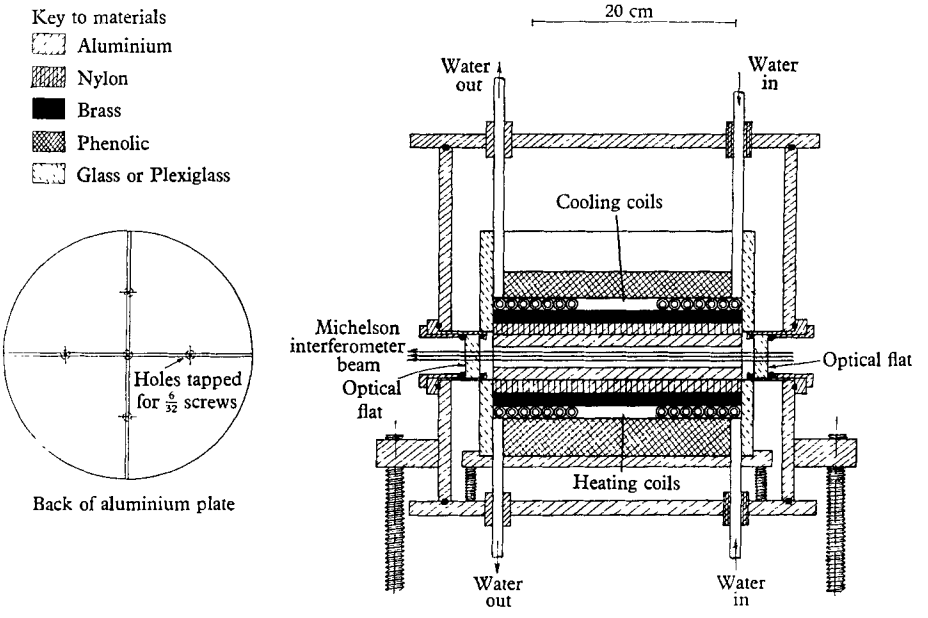

FIGURE 11. The convection cell (drawing in correct proportions).

Temperatures were measured by means of copper-constantan thermocouples made from 24-gauge wire. The couples were attached to screws of brass or aluminium, depending upon the material of the plate in which they were inserted. The leads to the thermocouples in the aluminium plates were led away through grooves of minimum size on the surface facing the brass plates. According to the manufacturers, the probable departure from the National Bureau of Standards (1955*b*) thermal e.m.f. data is 0·44 %. When measured against a bath of crushed ice, a typical laboratory temperature should have an absolute accuracy of 0·1 °K, while errors in temperature differences should be smaller than errors from other causes. From *in situ* measurements under isothermal conditions, and from measurements on the detached thermocouples at a variety of temperatures, we were assured that their readings corresponded to within 0·01 °K, and that stray e.m.f.'s were negligible.

One thermocouple was mounted in the centre of each brass plate, and four in the aluminium plates (see insert, figure 11). No difference of temperature could be detected between the different points in the two aluminium plates, indicating that heat flux lines do not diverge over a large central area of the plate, even though some distortion is to be expected at the edges. As far as measurements of the onset of convection are concerned, the outer sections of the plate may be

regarded as a guard ring. Optical temperature measurements which explore a complete diameter (see §6.3) will, however, be influenced by distortion at the edges to an extent which it is hard to predict *ab initio*.

Gas pressures in the sealed compartment could be varied from a few mmHg to about 110 cmHg. The compartment was evacuated with a vacuum pump and slowly filled with air through a tube of Drierite, or ammonia directly from dry cylinder gas.

6.2. *Measurement of flux and emissivity*

Let us number the brass and aluminium plates 1, 2, 3, 4, commencing with the lowest brass plate. The flux, which is constant through the system, can be written

$$F = -\frac{\Delta\theta_{12}}{h_{12}}K_{12} = -\frac{\Delta\theta}{h}K_{\text{eff}} = -\frac{\Delta\theta_{34}}{h_{34}}K_{34}, \tag{30}$$

where quantities without numerical suffices refer to the gas-filled section, and the suffices (12) and (34) refer to the nylon plates. By reducing h to zero we may measure the ratio $K_{12}h_{34}/K_{34}h_{12}$, which was found to be $0{\cdot}850 \pm 0{\cdot}026$. We are not quite clear why the nylon disks differ so greatly from one another, but the difference was confirmed from decay-time measurements of a temperature perturbation.

In order to eliminate symmetrical heat leakage errors we used the average flux through the two nylon disks as a measure of the flux. The effective conductivity of the air or ammonia was, therefore, taken to be proportional to

$$S = \frac{\Delta\theta_{12} + 0{\cdot}85\Delta\theta_{34}}{\Delta\theta}. \tag{31}$$

According to expectation S for air should depend neither upon pressure, nor upon the direction ($S\uparrow$ or $S\downarrow$) of the heat flux, provided that convection does not take place. However, when upward and downward flux measurements were compared, differences of about 4·6 % were observed, although the average value

$$\bar{S} = \tfrac{1}{2}(S\uparrow + S\downarrow) \tag{32}$$

was independent of pressure. We take this to indicate asymmetry in the heat leakage, but by applying a correcting factor averaging to 0·977 to $S\downarrow$ or a factor averaging 1·023 to $S\uparrow$ we should have a measure of $\bar{S}$ whose accuracy is close to ± 1 %.

We can now write

$$\bar{S} = fK_{\text{eff}}/h. \tag{33}$$

Since dry air has no absorption bands in the infrared spectrum we see from (28) and (29) that

$$K_{\text{eff}} = K + \frac{\pi Q\epsilon h}{2-\epsilon}. \tag{34}$$

Since K is known for air, measurements of $\bar{S}$ for $h = 2$ cm and 5 cm enable us to determine ϵ and f independently. In order to compare results at slightly different temperatures we have reduced Q and K to 298·2 °K on the basis of $Q \propto \theta^3$, and the kinetic theory result $K \propto \theta^{\frac{1}{2}}$.

There results from the flux data in figure 15 (if the conductivity is assumed to be known exactly) $f^{-1} = 7{\cdot}85 \pm 0{\cdot}06 \times 10^3\ \mathrm{erg}^{-1}\ (^\circ\mathrm{K})^{-1}$, and $\epsilon = 0{\cdot}370 \pm 0{\cdot}005$; the uncertainties, being those associated with our measurements, should be compounded with uncertainties in the value of K for air.

The temperature profiles which are reported in §7.1 were measured more than a year after the convection measurements. At this time we found

$$\epsilon = 0{\cdot}417 \pm 0{\cdot}010,$$

and a value for f which did not differ significantly from that already quoted. This change accompanied a steady deterioration of the finish on the aluminium plates from the original polish.

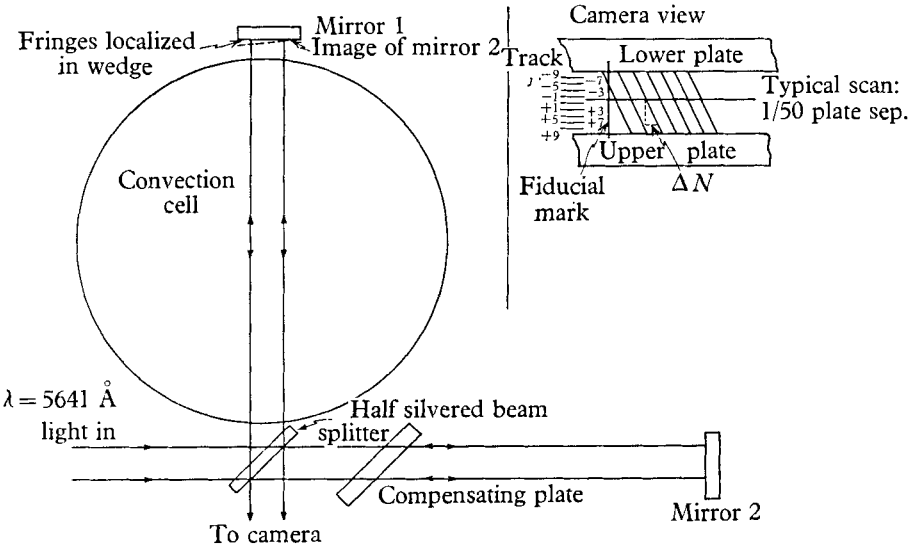

FIGURE 12. Lay-out of the interferometer.

6.3. *The Michelson interferometer*

In order to measure the vertical temperature profile the working section was placed in one arm of a Michelson interferometer (see figure 12 for details). The light rays passed through two optically flat windows which were placed as close as possible to the working section to minimize end effects.

Other experiments (e.g. Kennard 1941; Croft 1958) have employed interferometric methods to measure temperature profiles. The main source of error lies in variable end effects, which can only be assessed by measurements under circumstances in which the temperature profile is known. We have made use of the linear, diffusive profile in air between plates at known temperatures to determine these errors.

The interferometer was adjusted to give wedge fringes, located close to the Michelson mirrors. They were photographed by a camera focused on the far edge of the working section in order to yield a sharp image of the upper and lower surfaces. A vertical plumb bob at the camera focus in the reference arm provided a fiducial mark.

The interferometer was extemely sensitive to disturbances from road and subway traffic. A rigid table of honeycomb construction made from $\frac{1}{4}$ in. sheets of aluminium alloy was mounted on a deep independent footing in a basement. Individual optical elements were fixed with great rigidity to the table. Even with these precautions occasional vibrations disturbed the observations. Further disturbances were caused by temperature fluctuations in the open sections of the interferometer, and to record clear fringes short exposures were necessary. Since a very small aperture had been used in order to keep the beam divergence to an acceptable minimum, we were obliged to employ fairly fast plates (Kodak,

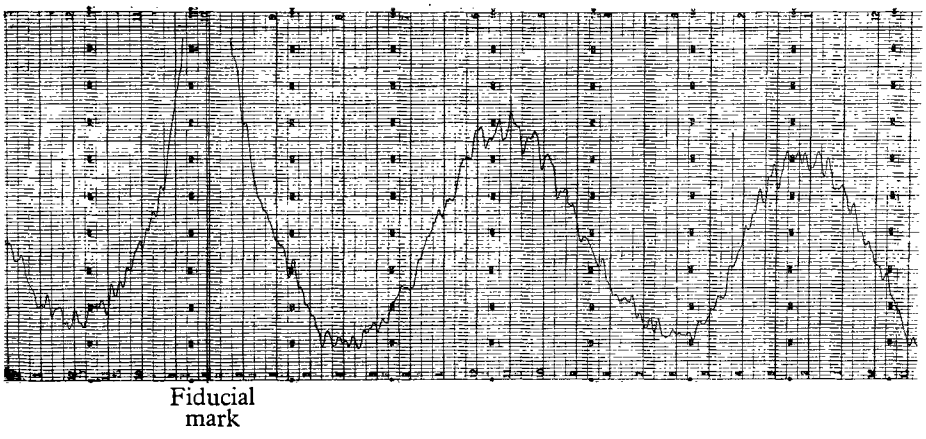

FIGURE 13. Microphotometer trace of fringes.

Metallographic). The axes of the various optical components of the interferometer had to be aligned with the convection cell with great accuracy to avoid excessive averaging of the temperature profile. A certain amount of space averaging occurred due to vertical spreading of the beam and mirage type refraction in the radiative-diffusive boundary layers, but we were able to demonstrate that this gives rise to no important errors.

Interferograms with air or ammonia in the working section were preceded and followed by interferograms with an evacuated working section. Typical photographs are shown in figure 21, plate 1.

The fringes were measured on a microphotometer. The space between the plates is divided into 20 equal parts by nineteen sections labelled $j = 0, \pm 1, \pm 2, \ldots \pm 9$, and scans were made at $j = \pm 1, 3, 5, 7$ and 9. A typical trace is shown in figure 13. Fringe shifts with respect to $j = -1$ could be estimated visually by superimposing microphotometer records, and matching several pairs of fringes independently to yield both a mean and a probable error. By subtracting the vacuum fringe positions, all characteristics of the optical system are eliminated. There was no difficulty in practice in deciding how many whole fringe shifts were involved in each case (a typical value of $\Delta\theta = 7\,^{\circ}\mathrm{K}$ corresponds to about 6 fringes for air at S.T.P.).

If N_j is the fringe shift at the j section, we measure $(N_j - N_{-1})$. We now form the average

$$\overline{N_j - N_0} = \tfrac{1}{2}\{(N_j - N_{-1}) - (N_{-j} - N_{-1})\}. \tag{35}$$

Let us expand $(N_j - N_0)$ in a series

$$(N_j - N_0) = a + bj + cj^2 + dj^3 + \ldots. \tag{36}$$

Then

$$\overline{N_j - N_0} = bj + dj^3 + \ldots. \tag{37}$$

We expect the temperature profile $(\theta_j - \theta_0)$ to be symmetrical and hence to contain no even terms in j. We may write

$$(N_j - N_0) = 2C(\rho_j l_j - \rho_0 l_0)/\lambda, \tag{38}$$

where C differs between air and ammonia, λ is the wavelength, and l_j the optical path. Since density is not simply proportional to temperature there are even terms in the expansion (36); there will be additional even terms if the effective optical path varies across the working section. By working with the mean value (35), we simultaneously eliminate all even terms, whether real or erroneous. Thus, we have

$$\overline{N_j - N_0} = \frac{2C\rho_0 l_0}{\lambda}\left(\frac{1}{\rho}\frac{\partial \rho}{\partial \theta}\right)_0 (\theta_j - \theta_0) + O[(\theta_j - \theta_0)^3] + \ldots. \tag{39}$$

We have been able to demonstrate that the second term on the right-hand side of (39) is negligible. With dry air at 1 atm. pressure we know that $(\theta_j - \theta_0)$ should be proportional to j. We have formed the partial regression of $\overline{N_j - N_0}$ on j and j^3, and find the cubic term to be insignificant. From the linear regression coefficient we find

$$l_0(\text{air, } 76{\cdot}05\text{ cmHg}) = 23{\cdot}86 \pm 0{\cdot}07\text{ cm}.$$

Since the plates have a diameter of 25·34 cm, this represents an important end-correction.

When this value of l_0 was applied to our results for ammonia we found a significant misfit at the boundaries, indicating a different l_0 for ammonia. Since, for ammonia, we know $\theta_{10} - \theta_0$ only, while the nearest measured quantity is $\overline{N_9 - N_0}$, extrapolation is necessary in order to make a comparison. This extrapolation was based on the theoretical profiles discussed in §4. From (39) there results

$$l_0(\text{NH}_3, 53{\cdot}0\text{ cmHg}) = 24{\cdot}31 \pm 0{\cdot}24\text{ cm},$$
$$l_0(\text{NH}_3, 98{\cdot}3\text{ cmHg}) = 24{\cdot}38 \pm 0{\cdot}12\text{ cm}.$$

7. Results and discussion

7.1. *Temperature profiles*

In figure 14 good agreement is demonstrated between theory and experiment. Each profile is the mean of three independent measurements. With sufficient care we were able to reduce random errors to about $\pm 0{\cdot}02$ °K. Since, on the average, one degree corresponds to about one fringe, we claim a precision of about 1/50 fringe. No great improvement in this precision is likely to be achieved without considerable effort.

While these experiments confirm the validity of the theory and while they give encouragingly small random errors, systematic errors due to uncertainty in l_0 give rise to serious restrictions on the value of the interferometric method for the investigation of unknown profiles. The difference between l_0 for air and

ammonia is about 2 %. If, for example, l_0 were unknown for air and the value for ammonia were employed, the experimental points would cluster around the broken line in figure 14, rather than around the ordinate. Such an error would largely destroy a claim to agreement between measurement and theory. For a less well understood temperature profile, such as that for fully-developed thermal turbulence, the extrapolation to $j = 10$ would be difficult to perform as precisely as we have been able to do.

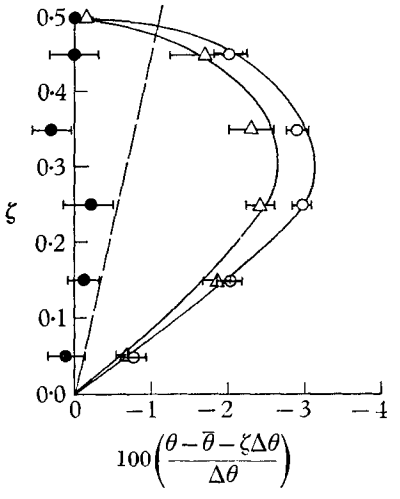

FIGURE 14. Temperature profiles in air and ammonia. Plate spacing 1·987 cm; $\Delta\theta = +7$ °K. The full lines are computed. The points are measured and the horizontal lines indicate the probable errors. $l_0(NH_3) = 24{\cdot}36$ cm; l_0(air) = 23·86 cm; $\epsilon = 0{\cdot}417$. (●) $p_{air} = 76{\cdot}05$ cmHg, (△) $p_{NH_3} = 53{\cdot}00$ cmHg, (○) $p_{NH_3} = 98{\cdot}33$ cmHg. The broken line is explained in the text.

7.2. *Heat flux*

Figure 15 shows the parameter $\bar{S}$ for air (equation (32)) as a function of pressure. Neither radiative nor diffusive flux is expected to vary with pressure, and a horizontal line of best fit has, therefore, been employed.

An altogether different picture is presented by the ammonia results shown in figure 16. Although the scatter of points is somewhat larger than for air, a significant increase of heat flux with pressure is demonstrated for both 2 and 5 cm plate separations. The theoretical curves fit the results well, although, since the intercept at $p = 0$ has been chosen for best fit, the significance of this result is not great.

The intercept can yield values for the conductivity of ammonia. For 2 cm we find a value 0·9 % below that quoted in §3; for 5 cm the value is low by 7·8 %. We attribute these discrepancies to the existence of edge effects, which are larger for 5 cm than for 2 cm spacing. By this token, of course, our method of computing f and ϵ from the results for air may be in error. We have not attempted to investigate this point at length, because our technique is essentially one of comparing the behaviour of air and ammonia; we are entitled to assume that edge effects are similar for the two gases.

This result suggests that edge effects are small for 2 cm, but may amount to a few percent for 5 cm, and this factor should be borne in mind when comparing theoretical and observed data for the onset of convection.

The main significance of our theoretical curves is that they provide a basis for making a best fit to the observed data. The best fit for $\epsilon = 0{\cdot}37$ is used in §12 to define the pre-convective condition in ammonia.

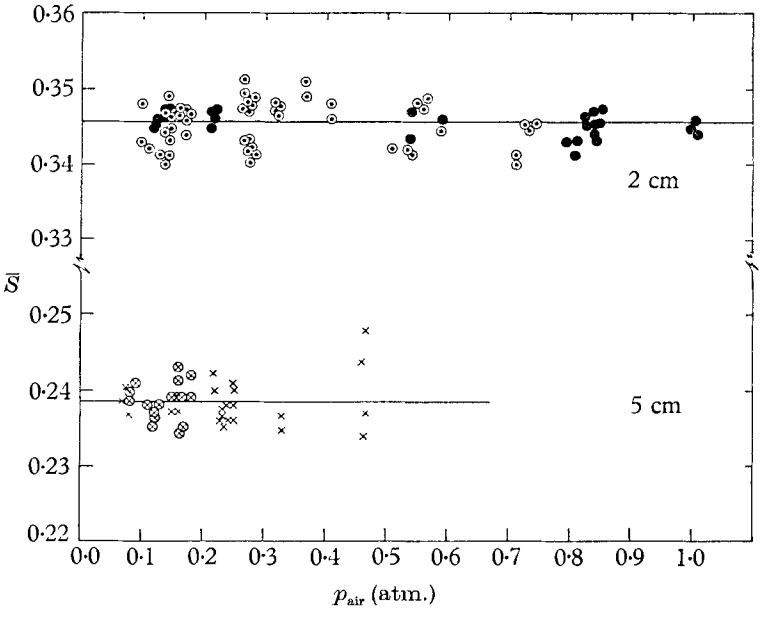

FIGURE 15. Heat flux for air as a function of pressure. (●) plate spacing 1·987 cm; (×), plate spacing 5·048 cm. Ringed points are for upward fluxes.

8. The onset of convection

If the lower plate is at the higher temperature, and if the temperature difference is sufficiently large, the enclosed gas will become unstable to small disturbances, and convection will start. For a non-radiating gas, such as air, in which the static state is a constant temperature gradient, the stability condition for rigid and conducting boundaries is

$$Ra = -\frac{g\alpha\beta h^4\rho^2 c_p}{K\eta} < Ra_c(\text{diff}) = 1708,$$

where g is the acceleration of gravity.

Goody (1956) and Spiegel (1960) have treated the problem of convection in a grey radiating gas. Both showed that radiation stabilizes the fluid, by offering a means of damping temperature fluctuations in addition to thermal diffusion. Further stabilization results from the thermal boundary layers created by radiative effects (see §4). By concentrating gradients near to the boundaries the bulk of the fluid is stabilized, and the critical Rayleigh number increased. These two stabilizing effects are separable, at least to the degree of approximation that critical Rayleigh numbers are usually computed.

The foregoing statement can be justified either in terms of the variational technique established by Pellew & Southwell (1940) or in terms of Chandrasekhar's (1961) treatment. In this particular case the results of the two methods are

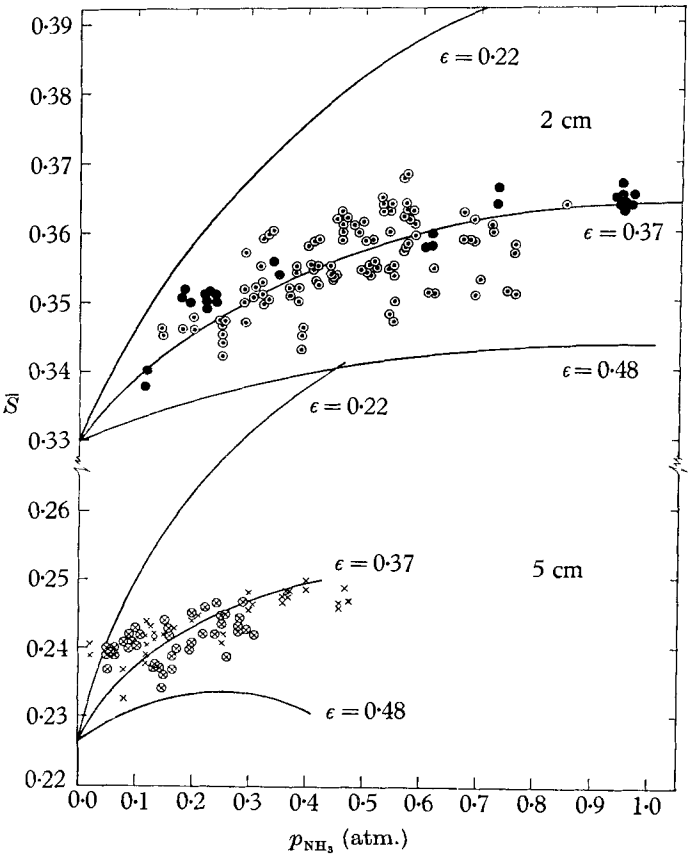

FIGURE 16. Heat flux for pure ammonia as a function of pressure. (●), plate spacing 1·987 cm; (×), plate spacing 5·048 cm. Ringed points are for upward fluxes. The lines are taken from figures 9 and 10.

identical, both in demonstrating the nature of the separability and in its actual magnitude. Following Pellew & Southwell (see also: Spiegel 1960; Goody 1956; Goody 1964), we may write

$$Ra_c = \frac{h^2}{K} \frac{\mathscr{M}[\mathscr{H}[\{(D^2-a^2)^2/a^2\}\omega]]}{\mathscr{M}[(\beta/\bar{\beta})\omega]}, \tag{40}$$

where $\mathscr{M}$, $\mathscr{H}$ and $(D^2-a^2)^2/a^2$ are linear operators, and ω is the unknown vertical velocity component. The operation $\mathscr{H}$ relates the heating rate (from both modes of heat transfer) to the entire temperature structure, see equation (23)

$$H = \mathscr{H}[\theta]. \tag{41}$$

The operator $\mathscr{M}$ is chosen to satisfy a variational principle whereby errors in ω will result in lower-order errors in Ra_c. If a suitable operator can be found it is usually enough to employ a guessed trial function ($\omega^{(0)}$, which must, however, obey the boundary conditions) in order to obtain a satisfactory estimate of Ra_c.

With this formulation we may write

$$Ra_c/Ra_c(\text{diff}) = S_\beta S_H, \tag{42}$$

where

$$S_\beta = \mathscr{M}[\omega^{(0)}]/\mathscr{M}[(\beta/\bar{\beta})\,\omega^{(0)}] \tag{43}$$

depends upon the boundary conditions, the trial functions, and the initial temperature profile, but not directly on the heat transfer mechanism, while

$$S_H = \{Ra_c(\text{diff})\}^{-1}\frac{h^2}{K}\frac{\mathscr{M}[\mathscr{H}[\{(D^2-a^2)^2/a^2\}\omega^{(0)}]]}{\mathscr{M}[\omega^{(0)}]}, \tag{44}$$

gives the stabilization caused by additional modes of heat transfer for an initial state with a constant temperature gradient.

9. The effect of the initial static state

According to Spiegel (1960), the operator

$$\mathscr{M}[\ ] = \int_{-\frac{1}{2}}^{\frac{1}{2}} [\ ](D^2-a^2)^2\,\omega^{(0)}\,d\zeta \tag{45}$$

gives a satisfactory variational principle for combined radiative and diffusive heat transfer provided that β is constant. Equation (45) cannot be used exactly as it stands for the case of variable β, but a first approximation using Chandrasekhar's technique leads precisely to (43) and (45) and these will be used to determine S_β.

According to Chandrasekhar a suitable trial function for rigid boundaries is

$$\omega^{(0)} = (\pi^2+a^2)^{-2}\left\{\cos\pi\zeta - \frac{\pi}{a+\sinh a}\sinh\tfrac{1}{2}a\cosh a\zeta + \frac{2\pi\zeta}{a+\sinh a}\cosh\tfrac{1}{2}a\sinh a\zeta\right\},$$

$$(D^2-a^2)^2\,\omega^{(0)} = \cos\pi\zeta. \tag{46}$$

This trial function corresponds to the largest scale of motion that can be developed in the body of the fluid, which is the least stable convective mode. a is an adjustable parameter with respect to which the critical Rayleigh number should be minimized. Its value for convection in a non-radiating fluid is $a \simeq \pi$; we will adopt this value because S_β depends but slightly upon it.

Substituting equations (24), (45) and (46) in (43), we find, after lengthy algebraic manipulations,

$$S_\beta = (A + 0{\cdot}013B - 0{\cdot}0008C)^{-1}. \tag{47}$$

In §4 we computed A, B and C for all conditions of importance to this paper. The most non-linear profile was for $h = 5\,\text{cm}$, $p_{\text{NH}_3} = 0{\cdot}4\,\text{atm.}$, for which

$$A = 0{\cdot}7722, \quad B = 0{\cdot}5204, \quad C = 14{\cdot}7544.$$

Substituting these figures in (47) we find $S_\beta = (0{\cdot}763)^{-1}$ which, to the accuracy of our experiments, cannot be distinguished from $(A)^{-1}$. We therefore conclude that for the conditions of our experiments it is sufficient to write

$$S_\beta = A^{-1}, \tag{48}$$

that is, to replace the mean temperature gradient in the computed Rayleigh number by the gradient in the central region of the fluid.

10. The effect of radiative heat transfer

Equation (22) relates the radiative heating rate to the temperature field for a stratified fluid in which temperature varies only in the vertical direction. The operator $\mathscr{H}$ must be valid for a three-dimensional disturbance, however, and its radiative part would be exceedingly complicated. $\mathscr{H}$ could, in principle, be written down and substituted in (44) to give a complete approximate expression for Ra_c. The numerical work would however be extensive, even if a useful method of solution could be found, and we have therefore preferred a less precise approach based upon a dimensional argument.

Convection develops in a fluid when the work done by buoyancy forces exceeds that required to overcome friction. Buoyancy forces are destroyed by both diffusive and radiative dissipation, and we may conjecture the existence of a characteristic time of dissipation (τ).

Since H has the dimensional form $\rho c_p[\theta][\tau]^{-1}$, we may infer from (41) that

$$\mathscr{H} \sim \tau^{-1}, \tag{49}$$

and hence, from (44)

$$S_H = \tau(\text{diff})/\tau. \tag{50}$$

Spiegel (1960), by means of a more detailed argument, reaches this same conclusion.

If radiation and diffusion act together, we may reasonably expect that

$$\tau^{-1} = \tau^{-1}(\text{rad}) + \tau^{-1}(\text{diff}), \tag{51}$$

and therefore

$$S_H = 1 + \tau(\text{diff})/\tau(\text{rad}). \tag{52}$$

If this approach is to be of value, the ratio $\tau(\text{diff})/\tau(\text{rad})$ should not greatly depend on the nature of the disturbance. Let us therefore evaluate the ratio for an infinite harmonic disturbance of wavelength $2\pi l$. For diffusion alone, we have the well-known result

$$\tau(\text{diff}) = (\rho c_p/K)\, l^2. \tag{53}$$

Spiegel (1957) has obtained the comparable solution for a grey absorbing gas, and this has been extended to a non-grey gas by Goody (1964) along lines suggested by the work of Townsend (1958). The result is

$$\tau(\text{rad}) = \frac{4\pi Q}{\rho c_p}\,\tilde{k}(l), \tag{54}$$

where

$$\tilde{k}(l) = \int_0^\infty \mathscr{E}'(r)\left\{\frac{\sin(r/l)}{r/l} - \cos(r/l)\right\}\frac{dr}{r}.$$

The grey solution is a special case,

$$\tilde{k}(l) = k\left\{1 - kl\tan^{-1}\left(\frac{1}{kl}\right)\right\}. \tag{55}$$

In figure 4 we presented data for $\mathscr{E}'(r)$. A comparatively simple numerical quadrature is involved in evaluating $\tilde{k}$ from equation (54). We find approximately that

$$\tilde{k}(l) \simeq \mathscr{E}'(1{\cdot}5l). \tag{56}$$

More precise data are given in figure 17.

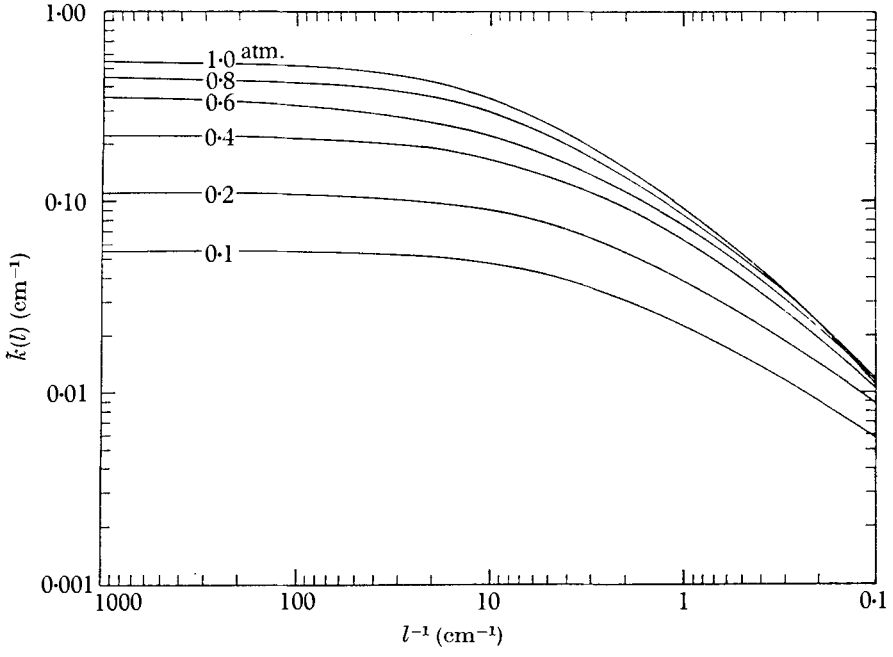

FIGURE 17. $\tilde{k}$ for ammonia.

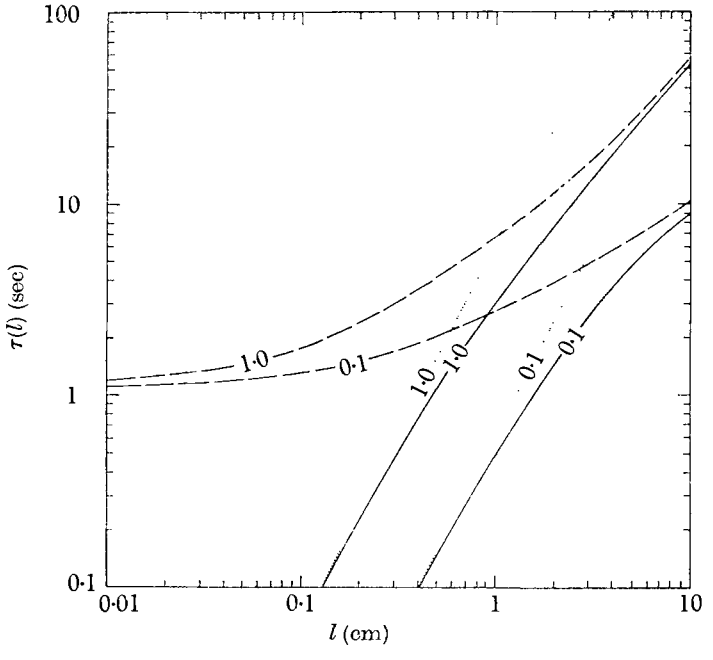

FIGURE 18. Characteristic time constants in ammonia. Pressures of ammonia in atmospheres are marked on the curves. ... τ(diff), from (53); – – – τ(rad), from (54); —— τ, from (51).

Some computed time constants are shown in figure 18. It is clear that considerable stabilization is to be expected for scales of a few centimetres, but it remains to relate the scale, l, to the characteristic scale for the experiment, which is the plate spacing, h.

Since convection cells are generally considerably wider than high, there is no obvious relation between l and h. We may reasonably assume proportionality, however,

$$l = h/b, \tag{57}$$

and seek an optimum value for the constant b. We note that the value of b is unimportant when diffusion dominates, and therefore we should seek the best value when radiative control is strong.

Spiegel (1960) has given a complete numerical solution for rigid boundaries when radiative transfer completely dominates diffusive transfer. The solution is for a grey absorption coefficient and we may compare the stability with that which results from expressions (52), (53) and (55). Table 3 shows a comparison between numerical and dimensional solutions for $b = 5{\cdot}0$; the agreement is as close as might be expected in view of the errors of the numerical solution.

	Ra_c/χ	
kh	Numerical	Equation 56, $b = 5{\cdot}0$
0	0	0
0·1	2·01	1·99
0·5	44·9	43·7
1	155	149
π	749	739
5	1081	1100
10	1440	1488
1000	1716	1708

TABLE 3. Comparison of dimensional theory and numerical calculations.

11. Convection in dry air

The apparatus described in §6.1 was used to determine the critical Rayleigh number. The plate spacing was either 5·048 cm or 1·987 cm and the temperature difference between the aluminium plates was then set to one of two temperatures (1·8 and 6·0 °K for 5 cm spacing or 2·8 and 6·3 °K for 2 cm spacing). The pressure cell was evacuated, and a long period of time was allowed to elapse in order to achieve a steady state. The plate temperatures were measured, and the quantity $\bar{S}$ (§6.2) was computed. The air pressure was then increased, and after a relatively short time interval temperatures were again measured. The Rayleigh number varies as (pressure)^2 and varying the pressure, therefore, provided a convenient means of changing the Rayleigh number, while at the same time making only a trivial change in the thermal conditions.

The data for low pressures (low Rayleigh numbers and, therefore, non-convecting) have already been discussed in §6.2. $\bar{S}$ should not vary with Rayleigh

number, and calibration constants were determined from the mean of all measurements in the conductive régime.

For $R > R_c$, however, $\bar{S}$ increases with Rayleigh number, as shown in figure 19. When $\bar{S}$ exceeded the value for the conductive régime by more than twice the estimated standard deviation of a single point, it was assumed that convection had started.

In the convective régime, approximate proportionality is exhibited between $\bar{S}$ and Ra. However, we do not know the shape of the curve *a priori* and hence, we made a best fit to the quadratic expression

$$Ra = Ra_c + b(\bar{S} - \bar{S}_0) + c(\bar{S} - \bar{S}_0)^2, \tag{58}$$

where $\bar{S}_0$ is the mean value of $\bar{S}$ for the conductive régime.

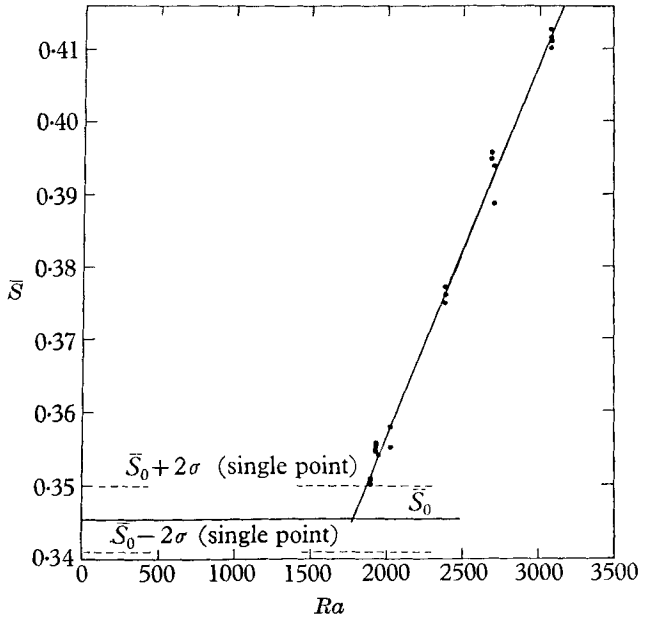

FIGURE 19. $\bar{S}$ as a function of Rayleigh number for dry air.
$h = 1{\cdot}987$ cm, $\Delta\theta = -5{\cdot}9$ °K.

Ra_c, b, c and the standard deviations σ_{Ra_c}, σ_b, σ_c were estimated by the method of least squares. While c did not differ significantly from zero, the inclusion of the term considerably increased the standard deviation of Ra_c. The uncertainty could be decreased by determining mean values of c and σ_c from all results taken together, and re-determining the best fit to equation (58) using these values.

The overall mean value of Ra_c from Table 4 is 1786 ± 16. There is no strong evidence that the critical Rayleigh number varies either with temperature difference or with plate spacing, although the errors for 5 cm spacing are large and the test is not very discriminating.

As far as we are aware, this is the first attempt that has been made to determine the critical Rayleigh number of a gas with precision. Sutton (1951) reports unpublished work by Dassanayake, but no experimental details are offered.

Otherwise, all precise determinations (e.g. Malkus 1954; Silveston 1958) have been for liquids, and work on gases has been of a qualitative nature only.

Our measured value of Ra_c differs significantly from the theoretical value of 1708 for rigid surfaces. The discrepancy is about 4·6 %, and at least two explanations are available. It is within the uncertainty of our knowledge of the fundamental data, η and K. If this is the explanation, measurements of the critical Rayleigh number could provide a means of improving our knowledge of these basic data. It is, however, a lengthy and difficult technique compared to conventional methods. Alternatively, we may have some effect from a horizontal

Run	$-\Delta\theta$[(1)] (°K)	h (cm)	Ra_c[(2)]	p_c[(3)] (cmHg)
1	~ 5·7	5·048	1738 ± 163	11·9
2	~ 6·1	5·048	1755 ± 157	11·3
Mean (1, 2)[(4)]	~ 5·9	5·048	1747 ± 113	11·6
3	~ 1·75	5·048	2042 ± 190	21·8
4	~ 1·75	5·048	1568 ± 552	21·3
Mean (3, 4)	~ 1·75	5·048	1992 ± 180	21·7
5	~ 2·85	1·987	1810 ± 32	68·8
6	~ 2·8	1·987	1761 ± 33	68·3
Mean (5, 6)	~ 2·8	1·987	1786 ± 23	68·6
7	~ 6·2	1·987	1828 ± 77	48·1
8	~ 5·9	1·987	1781 ± 24	47·8
Mean (7, 8)	~ 6·0	1·987	1785 ± 23	47·8

(1) $\Delta\theta$ differed slightly from point to point; precise values were used to calculate Ra.
(2) Standard deviations are given.
(3) Pressure when $Ra = Ra_c$.
(4) Means are weighted according to the standard deviation of Ra_c.

TABLE 4. Critical Rayleigh numbers for dry air.

quantization of cell size, imposed by the lateral boundaries, and constraining the critical Rayleigh number to be higher than its minimum value. Under the most favourable circumstances (h = 2 cm) our cell has a width to height ratio of 12·5. For rigid boundaries convection cells are twice as wide as they are high; hence, six cells will fill a diameter, of which the outer two are likely to be distorted. There is, therefore, good reason to expect some influence of the side walls on the critical Rayleigh number. This did not deter us in the initial design of the experiment since our object was to compare the behaviour of air and ammonia, for which the effects may be expected to be similar.

All runs were performed with pressure increasing with time with the exception of number 8 (table 4). That this run does not differ significantly from the mean of all runs indicates that there is no significant hysteresis at the critical point.

12. Convection in ammonia

Similar runs were performed with the convection cell filled with dry ammonia. The pre-convective data have already been discussed in §7.2. The theoretical curves shown in figure 16 were used to determine the onset of convection in all

runs. When the value of $\bar{S}$ exceeds that for the theoretical, pre-convective curve by twice the standard deviation of a single point, it was presumed that convection had started. Convective data were again fitted to solution (58), but the axes had to be rotated so that the pre-convective curve near to the onset point is parallel to the abscissa in order to reduce the calculation to a standard form.

Run	$-\Delta\theta$ (°K)	h (cm)	Ra_c	p_c (cmHg)
1	~ 5·8	5·048	2515 ± 572	11·9
2	~ 5·8	5·048	2999 ± 206	13·5
Mean (1, 2)	~ 5·8	5·048	2943 ± 194	13·0
3	~ 1·8	5·048	4947 ± 1604	30·1
4	~ 1·8	5·048	4795 ± 712	29·7
Mean (3, 4)	~ 1·8	5·048	4870 ± 651	29·8
5	~ 2·8	1·987	1955 ± 123	59·9
6	~ 2·8	1·987	2251 ± 208	64·3
7	~ 2·8	1·987	2454 ± 199	67·4
Mean (5, 6, 7)	~ 2·8	1·987	2125 ± 93	62·4
8	~ 6·4	1·987	2464 ± 62	46·4
9	~ 6·3	1·987	2793 ± 69	49·6
10	~ 6·4	1·987	2546 ± 104	47·5
11	~ 6·3	1·987	2241 ± 266	44·8
Mean (8, 9, 10, 11)	~ 6·4	1·987	2591 ± 42	47·7

For explanations see table 4. Note that means are weighted according to the number of degrees of freedom.

TABLE 5. Critical Rayleigh numbers for ammonia.

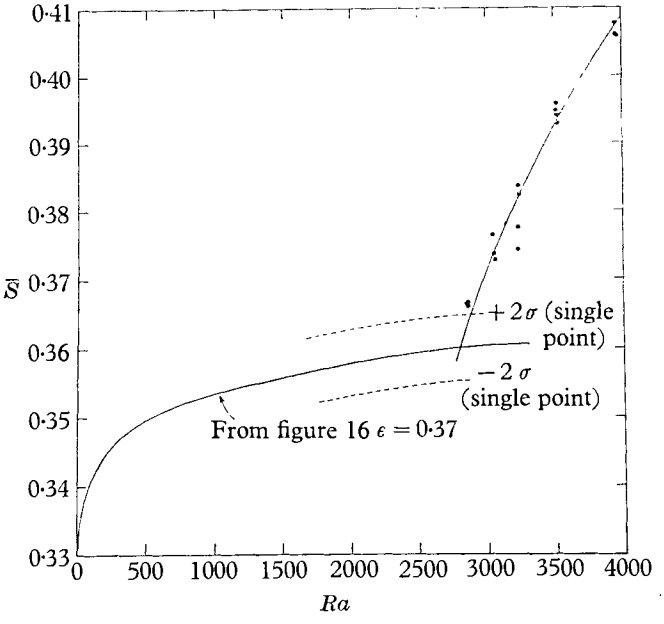

FIGURE 20. $\bar{S}$ as a function of Rayleigh number for ammonia.
h = 1·987 cm, $\Delta\theta$ = −6·3 °K.

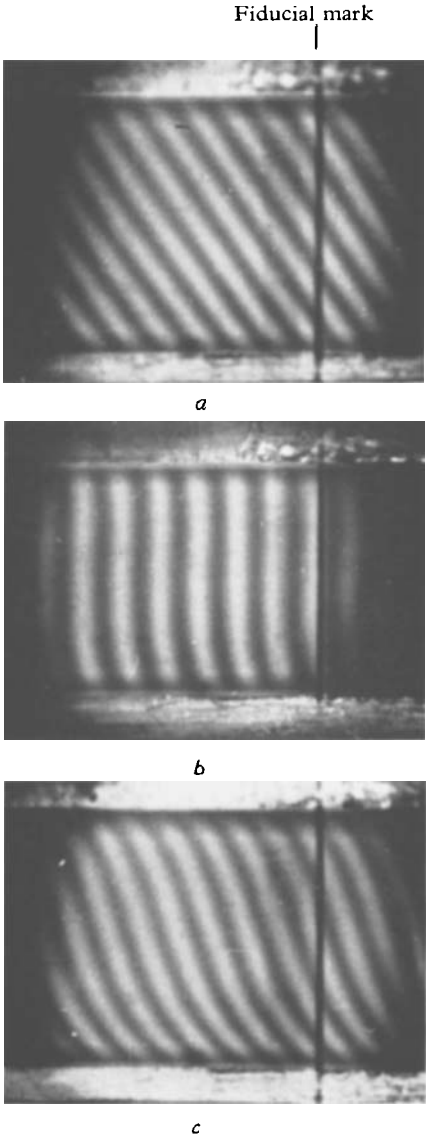

FIGURE 21. Interference fringes. (*a*) Air; $p = 76{\cdot}05$ cmHg; $\Delta\theta = +6{\cdot}85$ °K. (*b*) NH_3; $p = 53{\cdot}00$ cmHg; $\Delta\theta = +7{\cdot}26$ °K. (*c*) NH_3; $p = 98{\cdot}33$ cmHg; $\Delta\theta = +6{\cdot}79$ °K.

For ammonia we find significant values of the coefficient c, which differ from run to run. No attempt was, therefore, made to find a mean value, with the result that the uncertainty in Ra_c is larger than for air. Results are shown in table 5, and the experimental data for one run are shown in figure 20.

Table 5 shows large and significant increases in the critical Rayleigh number over the mean value for air (1786). This is in accordance with theory, since both S_β and S_H are necessarily greater than unity. A comparison of theoretical and observed stabilizations is given in table 6.

$-\Delta\theta$ (°K)	h (cm)	$\frac{Ra_c(NH_3)}{1786}$	S_β	S_H	$S_\beta S_H$
5·8	5·048	1·65 ± 0·11	1·22	1·33	1·62
1·8	5·048	2·73 ± 0·37	1·29	1·59	2·05
2·8	1·987	1·19 ± 0·05	1·13	1·25	1·41
6·4	1·987	1·45 ± 0·02	1·12	1·21	1·36

TABLE 6. Theoretical and observed stabilization.

13. Conclusions

The agreement between observed and predicted stabilizations shown in table 6 is good, but significant discrepancies exist. The significance of these discrepancies is decreased as we recognize an estimated uncertainty of about ± 0·07 in the theoretical stabilization, and the possibility of edge effects for 5 cm plate separation. These discrepancies are in any case not sufficient to cast doubt upon the basic theory, which is clearly confirmed by the experiment. The large amount of labour involved in obtaining precise results precluded a more extensive experimental investigation.

The overall picture is, however, one of good agreement between difficult measurements and an approximate theory. There is no doubt that we understand well the most important features of the problem of convective motion driven by radiative transfer. There need, therefore, be little hesitation in applying similar methods to planetary and stellar systems. Admittedly, this represents a very considerable extension of the theory, but it is rare indeed that astrophysical or geophysical phenomena can be tested on any scale.

While this result was our main objective, the investigation has been fruitful in other ways. We have been able to confirm, with reasonable accuracy, the validity of Rayleigh's theory for a non-radiating gas. More importantly, we have been able to make an objective test of methods used in atmospheric studies for computing a radiative-diffusive steady state. In the atmosphere it is very difficult to test theoretical results, which must largely be taken on trust. Agreement in a controlled laboratory situation is, therefore, a matter of considerable satisfaction.

We are indebted to the National Science Foundation for support of a programme of Atmospheric Physics at Harvard, to Mr Joachim Joseph for helping make the experimental measurements, and to Mrs Haydee Ern for assistance with the numerical computations.

REFERENCES

BENEDICT, W. S., PLYER, E. K. & TIDWELL, E. D. 1958 Vibration rotation bands of ammonia. I. The combination bands $\nu_2 + (\nu_1, \nu_3)$. *J. Res. N.B.S.* **61**, 123–147.

BLEANEY, B. & PENROSE, R. P. 1948 Collision broadening of the inversion spectrum of ammonia. III. The collision cross-section for self-broadening and for mixtures with non-polar gases. *Proc. Phys. Soc.* **60**, 540–549.

CHANDRASEKHAR, S. 1961 *Hydrodynamic and Hydromagnetic Stability*. Oxford: Clarendon Press.

CHAPMAN, S. & COWLING, T. G. 1952 *The Mathematical Theory of Non-Uniform Gases*. Cambridge University Press.

VAN CLEAVE, A. B. & MAASS, O. 1935 The variation of the viscosity of gases with temperature over a large temperature range. *Canad. J. Res.* **13**, 140–148.

CROFT, J. F. 1958 The convective region and temperature distribution above a horizontal heated surface. *Quart. J. R. Met. Soc.* **84**, 418–427.

FOLEY, H. M. & RANDALL, H. M. 1941 Fine structure in the far infrared spectrum of NH_3. *Phys. Rev.* **59**, 171–173.

FRANCK, E. U. 1951 Zur Temperaturabhängigkeit der Wärmeleitfähigkeit einiger Gase. *Z. Elektrochem.* **55**, 636–643.

FRIBERG, S. 1927 Über die Dispersion des Lichtes in gasformigen Körpern innerhalb des ultravioletten Spektrums. *Z. Physik*, **41**, 378–384.

GARING, J. S., NIELSEN, H. H. & RAO, K. N. 1959 The low frequency vibration-rotation bands of the ammonia molecule. *J. Mol. Spectroscopy*, **3**, 496–527.

GERHARD, S. L. & DENNISON, D. M. 1933 The envelopes of infrared absorption bands. *Phys. Rev.* **43**, 197–204.

GOODY, R. M. 1956 The influence of radiative transfer on cellular convection. *J. Fluid Mech.* **1**, 424–435.

GOODY, R. M. 1964 *Atmospheric Radiation. I. Theoretical Basis*. Oxford: Clarendon Press.

HADNI, A. 1953 Structure fine des raies de rotation de l'ammoniac de $J'' = 14$ a $J'' = 18$. *Compt. Rend., Paris*, **237**, 317–318.

HANSLER, R. L. & OETJEN, R. A. 1952 The infrared spectrum of HCl, DCl, HBr, and NH_3 in the region from 40–140 μ. *J. Chem. Phys.* **21**, 1340–1343.

HIRSCHFELDER, J. O., CURTISS, C. F. & BIRD, R. B. 1954 *Molecular Theory of Gases and Liquids*. New York: Wiley.

HOTTEL, H. C. 1954 *Heat Transmission*, ed. McAdams, W. H., Chapter IV. New York: McGraw-Hill.

KAPLAN, L. D. & EGGERS, D. F. 1956 Intensity and linewidth of the 15-micron CO_2 band, determined by a curve of growth method. *J. Chem. Phys.* **25**, 876–883.

KENNARD, R. B. 1941 Temperature distribution and heat flux in air by interferometry. *Temperature. Its Measurement and Control in Science and Industry*, pp. 685–706. New York: Reinhold.

LANDHOLT-BORNSTEIN 1962 *Zahlenwerte und Funktionen*, 1962, 6th edition. Berlin: Springer.

MASON, E. A. & MONCHICK, L. 1962 Heat conductivity of polyatomic and polar gases. *J. Chem. Phys.* **36**, 1622–1639.

MCKEAN, D. C. & SCHATZ, P. N. 1956 Absolute infrared intensities of vibration bands in ammonia and phosphine. *J. Chem. Phys.* **24**, 316–325.

NATIONAL BUREAU OF STANDARDS 1955*a* *Circular* 564. Tables of thermal properties of gases. Washington, D.C.: U.S. Department of Commerce.

NATIONAL BUREAU OF STANDARDS 1955*b* *Circular* 561. Reference Tables for Thermocouples. Washington, D.C.: U.S. Department of Commerce.

MALKUS, W. V. R. 1954 Discrete transitions in turbulent convection. *Proc. Roy. Soc.* A, **225**, 185–195.

OSBORNE, N. S., STIMSON, H. F., SLIGH, T. S., Jr. & CRAGUE, C. S. 1924 Specific heat of superheated ammonia vapor. *Sci. Papers Nat. Bur. Standards*, **20**, 65–110.

PELLEW, A. & SOUTHWELL, R. V. 1940 On maintained convective motion in a fluid heated from below. *Proc. Roy. Soc.* A, **176**, 312–343.

PIERSON, R. H., FLETCHER, A. N. & GANTZ, E. St. C. 1956 Catalogue of infrared spectra for qualitative analysis of gases. *Anal. Chem.* **28**, 1218–1239.

PORT, F. J., Jr. 1940 Heat Transmission by Radiation from Gases. Sc.D. Thesis, Dept. of Chemical Engineering, Massachusetts Institute of Technology.

SILVESTON, P. L. 1958 Wärmedurchgang in waagerechten Flüssigkeitsschichten. *Forsch. Ing. Wes.* **24**, 29–32 and 59–69.

SLAWSKY, Z. I. & DENNISON, D. M. 1939 The centrifugal distortion of axial molecules. *J. Chem. Phys.* **7**, 509–521.

SPIEGEL, E. A. 1957 On smoothing temperature fluctuations by radiative transfer. *Ap. J.* **126**, 202–207.

SPIEGEL, E. A. 1960 The convective instability of a radiating fluid layer. *Ap. J.* **132**, 716–728.

SUTTON, O. G. 1951 On the stability of a fluid heated from below. *Proc. Roy. Soc.* A, **204**, 297–309.

THOMPSON, H. W. 1941 The free energy of methyl cyanide and equilibrium constants of some related reactions. *Trans. Faraday Soc.* **37**, 344–352.

TOWNSEND, A. A. 1958 The effects of radiative transfer on turbulent flow of a stratified fluid. *J. Fluid Mech.* **4**, 361–375.

WRIGHT, N. & RANDALL, H. M. 1933 The far infrared absorption spectra of ammonia and phosphine gases under high resolving power. *Phys. Rev.* **44**, 391–398.